Available online at www.sciencedirect.com
SCIENCE DIRECT
Polymer 46 (2005) 10331–10338
polymer
www.elsevier.com/locate/polymer

Effect of short chain branching upon the crystallization of model polyamides-11

Stefano Acierno*, Peter Van Puyvelde

Department of Chemical Engineering, Katholieke Universiteit Leuven, W. de Croylaan 46, B-3001 Leuven, Belgium

Received 30 May 2005; received in revised form 21 July 2005; accepted 29 July 2005
Available online 1 September 2005

Abstract

In this paper, we study the effect of short (C7) branches on the crystallization behavior of model polyamides-11. The crystallization kinetics of samples with different amounts of branches are followed by differential scanning calorimetry, turbidity, and small angle light scattering measurements under both quiescent and shear-stimulated conditions. It is found that the presence of small amounts of C7-branches (<3 branches per 1000 atoms in the main chain) sensibly slows down the overall crystallization kinetics and the spherulitic linear growth rate. The application of relatively strong shear conditions (up to shear rates of 10 1/s and 60 strain units) does not provide any sensible increase of the crystallization kinetics and any modification of the spherulitic morphology.

Keywords: Crystallization; Polyamide-11; Rheo-optics

1. Introduction

Plastic products play a central role in life today with an application range that encompasses commodity household products as well as high-tech applications in the automotive, electronic, and medical industries. Despite of their widespread nature, the processing of such materials is not as straightforward as it might seem. In order to convert a polymer into a useful product, most polymer processes form a liquid polymer into the required shape using a die or a mould. However, this shape must be solidified, either in the mould or shortly after exiting from the die. These operations cause orientation and crystallization of the polymer molecules in the melt and will strongly influence the final polymer morphology [1–6]. In visualizing the effects of flow on the morphology evolution, many different parameters may contribute: the molecular architecture such as chain rigidity, chain branching, chain length and its distribution, as well as the efficiency of the orientation of the chains under the given processing flow.

In flow-induced crystallization, it is generally accepted that orientation of molecules in the flow direction promotes interactions of the chains [1–10]. The net result is an increase in the number of nuclei and in the crystallization kinetics. In order to fine-tune the end-use properties of the materials, the relation between molecular architecture and the flow-induced crystallization disserves significant attention [11]. Acierno et al. studied the effect of shear flow on the crystallization kinetics of several isotactic poly(1-butene) samples of different molecular weight. While the quiescent crystallization was found to be essentially M_w-independent [12], a strong effect of M_w on the flow-induced crystallization kinetics was observed [13]. The combined effect of flow and molecular weight could be cast in terms of a characteristic Deborah number (the shear rate times the characteristic relaxation time), which measures the ability of flow to orient the polymer chains. The proposed scaling was also able to explain qualitatively the observed transition from a low-shear isotropic morphology to a high-shear rate rod-like crystalline morphology. Similar observations were done by Elmoumni et al. on isotactic polypropylene samples [14].

One of the drawbacks of using commercial polymers in such studies is the inherent polydispersity in molecular

* Corresponding author. Address: Dipartimento di Ingegneria Chimica, Università degli Studi di Napoli Federico II, piazzale V. Tecchio 80, I-80125 Napoli, Italy. Tel.: +390 817682288; fax: +390 812391800.
E-mail address: sacierno@unina.it (S. Acierno).

0032-3861/$ - see front matter © 2005 Elsevier Ltd. All rights reserved.
doi:10.1016/j.polymer.2005.07.097

weight of the polymers. With the advent of metallocene catalysts for olefin polymerization, many structural features can be incorporated ad-hoc into polymer chains during polymerization [15,16]. This approach provides an opportunity to study the effect of well-defined molecular structures and to separate effects of molecular weight and its distribution on the flow-induced crystallization. From a rheological and a processing point of view, long-chain branches are considered to be of major importance, since they determine to a large extent the processability of the polymer due to their effect on the shear thinning and the elasticity of the material. In addition, these long-chain branches have a significant effect on the crystallization since their high relaxation time makes them suitable to act as nuclei. Agarwal et al. [17] studied the flow-induced crystallization of a new class of long-chain branched isotactic polypropylene synthesized using metallocene catalyst technology. It was shown that the enhancement in various mechanical properties, as well as the improved crystallization kinetics under flow, are due to the unique molecular structure that is coupled to the broadened and complex relaxation behavior with respect to the linear equivalent. On the other end of the molecular weight distribution spectrum, the importance of short chain branches (SCB) cannot be underestimated since they affect profoundly end-use properties such as stiffness, tear strength and clarity [18,19]. For instance, different degrees of SCB produce a wide variety of mechanical properties—ranging from rigid thermoplastics to elastic rubber-like materials—due to differences in the crystal morphology and the crystallinity.

It has been demonstrated that above a critical molecular weight of the branch the crystallinity decreases with increasing the branch length, due to the inability of the longer chains to be incorporated in the crystalline structure [20,21]. More significantly, by increasing the number of short-branches, the polymer crystallinity and density can be reduced, since these side chains do not crystallize and are rejected into the amorphous regions of the polymer [22,23]. A reduced density hence results in a higher flexibility and in an increased ability to absorb and dissipate energy [22–24].

Most often, studies on the effect of branching on crystallization are limited to polyolefines, probably due to the relative ease of which metallocene catalysis can be employed to modify the architectures. However, technical polymers such as aliphatic polyamides, commonly known as nylons, also occupy a prominent position in the realm of polymers. These are semi-crystalline polymers that usually exhibit a relatively high modulus, toughness and strength, low creep and good temperature resistance that allow a widespread use of this family of polymers as fibers and engineering thermoplastics. Experimental studies on the isothermal and non-isothermal crystallization of nylons are rather scarce in literature and are limited to the investigation of the crystal structure and the characterization of the Avrami parameters using differential scanning calorimetry [25–27]. According to our knowledge, no systematic studies on the effect of molecular architecture of polyamides on their crystallization behavior under quiescent and flow-stimulated conditions have been performed so far. This is not straightforward since long-term experiments on polyamides are not easy to be performed due to their hygroscopic nature [28,29]; when kept at high temperature for a long time (typically these conditions are met during the annealing phase preceding the crystallization experiments) post-condensation reactions take place thus altering the molecular weight of the sample [30]. In order to circumvent this problem, model polyamides with a higher thermal stability have been synthesized thus allowing for a sufficient experimental time window to perform crystallization experiments. More specifically, a series of polyamide-11 (PA11) with different amounts of short-chain branches have been prepared. The main chain length and the molecular weight distribution have been kept the same in order to investigate the net effect of the short chain branches. Both rheological as well as rheo-optical techniques are used to study the crystallization of these materials under quiescent and flow-stimulated conditions.

2. Experimental section

2.1. Materials

Since, the goal of the work is to study the effect of short branches on the crystallization, model polyamides-11, having similar backbone length and different, (well defined) amounts of short C7 branches, were synthesized. Mixtures of 11-aminoundecanoic acid and 11-heptylaminoundecanoic acid with, respectively, 0, 1 and 5 wt% of 11-eptylaminoundecanoic were employed for the syntheses, no catalyst was used in order to increase the thermal stability of the produced polymers and hence to enlarge the time window available for further rheological tests. Details about the polycondensation conditions can be found elsewhere [31]. The produced polyamides will be denoted further on in this paper as linear PA11, 1% C7 and 5% C7 in memory of the weight percentage of heptylaminoundecanoic used for the synthesis. It should be noted that these notations correspond to average densities of C7 branches of 0, 0.56 and 2.85 branches per 1000 atoms in the main chain.

The polymers discharged from the reactor were granulated and the as-produced pellets were conditioned in vacuo ($\sim$10 mbar) at 80 °C for 20 h in order to reduce the water content to less than 0.03 wt% prior to any further analysis.

The melting temperatures, defined as the peak temperature during a DSC endotherm at a heating rate of 10 °C/min, are given in Table 1. Some other physical properties of the PA11 samples are also given in Table 1.

Table 1
Some physical properties of the various PA11 samples

	Linear PA11	1% C7	5% C7
Branches/1000 atoms in the main chain	0	0.56	2.85
T_m (°C)	190.4	190.3	186.3
$[\eta]$ (ml/g)	151	157	135
M_w (g/mol)	51,500	55,100	42,500

2.2. Samples characterization

Intrinsic viscosity measurements in *m*-cresol (>99%) were performed in order to determine the molecular weight of the PA11 samples. The solutions were prepared following the recommendations of the ISO 307 standard. Polymer concentrations, c, ranging from 1 to 8 g/l were prepared by dissolving the polymers into hot (95 °C) *m*-cresol. The solutions were then filtered in a P100 grade sintered-glass filter and the flow times of the solvent ($t_{solvent}$) and solutions ($t_{solution}$) were measured at 25 °C using a Schott-Generate type II Ubbelohde viscometer. The reduced viscosity was calculated as:

$$\eta_{red} = \frac{1}{c}\frac{\eta_{solution} - \eta_{solvent}}{\eta_{solvent}} \simeq \frac{1}{c}\frac{t_{solution} - t_{solvent}}{t_{solvent}} \quad (1)$$

Results for the reduced viscosity vs concentration are shown in Fig. 1. A line (one for each sample) represents well the experimental data. The intercepts of the linear regressions represent the intrinsic viscosities and their values are reported in Table 1. The slope is not affected by the presence of short branches.

The intrinsic viscosity, in turn, is related to the polymer molecular weight through the well-known Mark–Houwink relationship whose coefficients can be found in literature [32]. The values for the molecular weights as calculated form the Mark–Houwink relationship are also reported in Table 1. The data suggest that the molecular weights of the different samples are quite similar; in particular the linear PA11 has a weight average molecular weight of about 51,500 g/mol, the 1% C7 has a molecular weight 7% higher while the 5% C7 has a molecular weight 18% lower.

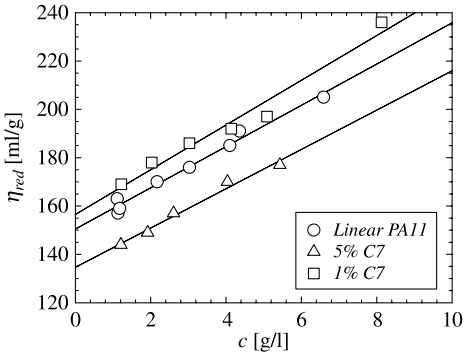

Fig. 1. Reduced viscosity vs concentration. Measurements have been performed in 99%-pure *m*-cresol at 25 °C.

2.3. Methods

Pre-dried polymer pellets were used for the experiments. Crystallization isotherms were preceded by an annealing phase of 5 min at 210 °C, these conditions were proven to be sufficient to provide reproducible results (even if a complete melting of the crystalline phase is not guaranteed).

The rheological experiments were performed with a stress-controlled rotational rheometer (SR-200 of Rheometric Scientific) equipped with disposable parallel plates (diameter 25 mm) and a gap thickness of 1 mm. All the measurements were carried out under a dry nitrogen atmosphere to minimize polymer degradation and moisture absorption. Viscoelastic measurements were performed in the frequency window 0.1–100 rad/s (4 points/decade) using a strain amplitude of 1–10%, in order to ensure sufficiently high torque values while remaining in the linear viscoelastic range. The processing of linear viscoelastic data was performed using the software IRIS (http://rheology.tripod.com).

The isothermal crystallization experiments followed an experimental protocol consisting of a preheating stage of the sample to 210 °C for 5 min and a cooling stage (−20 °C/min) to the test temperature. The zero of the time scale was assigned to the instant at which the crystallization temperature was reached.

The development of crystallinity was followed by differential scanning calorimetry (DSC), turbidity and small angle light scattering (SALS) measurements.

Calorimetric measurements were done using a Shimadtzu DSC60 instrument. Temperature and heat flux were calibrated using high purity indium and naphthalene. All DSC measurements were performed under dry nitrogen purge; samples weights were between 3 and 6 mg.

The SALS experiments were performed using a Linkam shearing cell (CSS 450 of Linkam Scientific Instruments) equipped with glass parallel plates; a sample thickness of 200 μm was used. The thermocouples of the Linkam cell were calibrated using the high-purity indium and naphthalene already used for the DSC instrument. The optical line used for the SALS experiments consisted of a linearly polarized laser light source (10 mW He–Ne, $\lambda = 632.8$ nm), a Glan-Thompson polarizer, a second polarizer, a screen and a highly sensitive (10 bits, 1300×1030 pixels) progressive scan CCD camera (Pulnix TM-1300). Image analysis was done using the homemade software SalsSoftware. Alternatively, during the turbidity measurements, the intensity of the transmitted light through the sample was measured by a photodiode detector, while the screen and the second polarizer were not used.

The flow-stimulated isothermal crystallization experiments were performed at the crystallization temperature of 180 °C. The shear flow was then imposed at the crystallization temperature applying different shear rates, $\dot{\gamma}$, and different shearing times, t_s, with the constraint of a constant applied shear strain: $\gamma = \dot{\gamma} \times t_s$. Two different values for the

strain, namely 6 and 60, were used. It was always verified that the shearing time was much smaller than the crystallization induction time.

3. Results and discussion

3.1. Rheological characterization

The rheological properties of the three PA11 melts were preliminary measured in the temperature range 190–210 °C. Such a narrow temperature range is due to the poor thermal stability of the samples at temperatures higher than 210 °C (see for example Acierno and Van Puyvelde [30]) and to the fast crystallization rates at temperatures lower than 190 °C. The linear viscoelastic data were reduced to the reference temperature of 210 °C by applying time-temperature superposition [33] and are reported in Figs. 2 and 3. Master curves of the moduli, at the reference temperature of 210 °C, are displayed in Fig. 2 where also moduli as calculated from a generalized Maxwell spectrum and the limiting slopes of 2 and 1 are added for comparison. Master curves of the complex viscosity are reported in Fig. 3.

As expected, the linear viscoelastic behavior of the three PA11's is typical of modestly entangled, linear polymer melts. In particular the terminal region is well visible, as confirmed by the limiting slopes of both elastic and loss moduli and by the plateau of the complex viscosity in the low frequency region.

The discrete relaxation spectrum (as calculated from the method of Baumgaertel and Winter [34] using the software IRIS) allows to calculate the zero-shear viscosity and the steady-state shear compliance according to the following formulas:

$$\eta_0 = \sum_1^N G_i \lambda_i \tag{2}$$

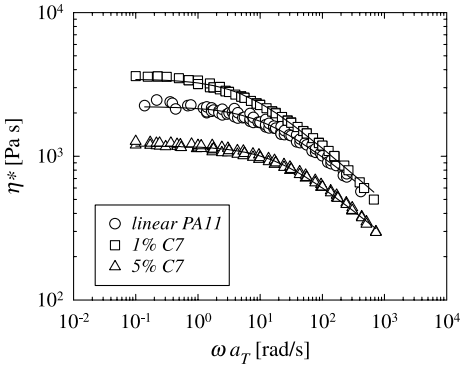

Fig. 3. Master curves of the complex viscosity at the reference temperature of 210 °C. The solid lines through data points are calculated from an Ellis viscosity equation.

$$J_e^0 = \frac{\sum_1^N G_i \lambda_i^2}{\left(\sum_1^N G_i \lambda_i\right)^2} \tag{3}$$

where G_i and λ_i are the initial modulus and the relaxation time corresponding to each Maxwell element. The characteristic relaxation time, defined as:

$$\lambda_c = \eta_0 J_e^0 \tag{4}$$

can be taken as a good estimate for the terminal relaxation time of the polymer. The values for the zero-shear viscosities, the steady-state shear compliances and the characteristic relaxation times as calculated at the reference temperature of 210 °C are given in Table 2.

As the zero-shear viscosity, for linear flexible polymers, increases with a 3.4 power of the molecular weight [33], differences in the zero-shear viscosity values can be related to differences in the molecular weight. From the linear viscoelastic characterization of the samples it can be deduced that the materials have similar molecular weights. In particular, the 1% C7 would have a molecular weight 15% higher than that of the linear PA11 while the 5% C7

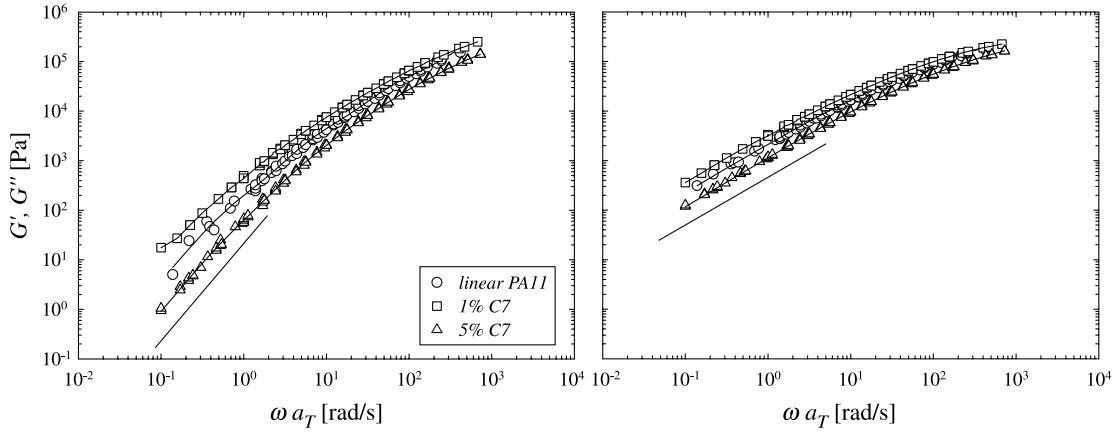

Fig. 2. Master curves of the storage modulus (on the left) and loss modulus (on the right) at the reference temperature of 210 °C. The solid lines through data points are moduli as calculated from a generalized Maxwell spectrum. The limiting slopes of 2 and 1 are also shown for comparison.

Table 2
Rheological parameters of the PA11's samples as calculated at the reference temperature of 210 °C

	Linear PA11	1% C7	5% C7
η_0 (Pa s)	2260	3610	1170
J_e^0 (10^5/Pa)	7.3	16	6.6
λ_c (s)	0.165	0.589	0.078
E/R (K)	8690	9060	9910

would have a molecular weight 18% lower with respect of the linear PA11. These values are in remarkably good agreement with the intrinsic viscosity results.

Both horizontal, a_T, and vertical, b_T, shift factors were calculated in the experimental temperature range. As expected the vertical shift factors are very close to unity and they weakly depend on the temperature; while the horizontal shift factors (not reported) show an Arrhenius-like behavior. Data regressions give the activation energies over the universal gas constant (which are also given in Table 2). The values obtained for the three samples are similar and the average value for the activation energy over the universal gas constant, E/R, is 9220 K.

Zero-shear viscosities and relaxation spectra provide a complete characterization of the linear viscoelastic behavior that, in view of the glass transition temperature of PA11 of about 42 °C and using the above calculated activation energies, can be shifted to the lower temperatures where the crystallization experiments are conducted and where the fast PA11 crystallization kinetics do not allow for the collection of linear viscoelastic data.

3.2. Quiescent crystallization

The quiescent crystallization kinetics for the three PA11 samples were determined by DSC experiments at the temperatures of 172.5, 174.6 and 176.7 °C. The specific heat flux vs crystallization time is reported in Fig. 4 where data sets corresponding to 174.6 and 176.7 °C are shifted vertically for the sake of clarity. From observation of Fig. 4 we deduce that for each temperature the linear PA11 sample is the fastest in crystallization while the 5% C7 sample is the slowest. A quantitative analysis of the data also suggests that the attained crystallinity decreases as the branching content increases, in particular crystallinities of 22, 19 and 17 wt% were calculated for the linear PA11, the 1% C7 and the 5% C7, respectively. The half-crystallization time ($t_{0.5}$, defined as the time taken to achieve a relative degree of crystallinity of 0.5) can be calculated from the DSC data. The half-crystallization time as a function of temperature (Fig. 9 further in this text) will be compared to the characteristic crystallization time as obtained from turbidity measurements.

The quiescent crystallization kinetics of the three PA11 samples at 176, 178, 180 and 182 °C were also followed by monitoring the intensity of the transmitted light through the sample and by depolarized small angle light scattering (V_H-scattering). Depolarized scattering indicates that the two polarizers are used in a crossed configuration. In Fig. 5 the time evolution of the relative intensity, I/I_0, for the 1% C7 sample at different temperatures is shown. The relative intensity is almost constant during a first time zone where the polymer remains essentially in the state of an undercooled melt. Then, as crystallization sets in, the nucleation and subsequent growth of crystallites generate a strong and relatively fast increase of the sample turbidity, which corresponds to a plain reduction of I/I_0.

In order to characterize quantitatively the overall crystallization kinetics, a half-turbidity time, ($\tau_{0.5}$, defined as the time where the transmitted intensity has decreased to 50% of its initial value for the first time) is used. It should be stressed that the choice of $\tau_{0.5}$ to characterize the crystallization kinetics is arbitrary and that no direct relation with the crystallization half-time $t_{0.5}$ should be deduced, as the sample turbidity is not a linear function of the degree of crystallinity.

All the relative intensity vs time curves show an evident minimum after which the intensity increases again. The presence of this minimum is linked to the changing scattering power of the system during crystallization. During the early crystallization stages the scattered light increases, then, as the spherulites impinge, the system

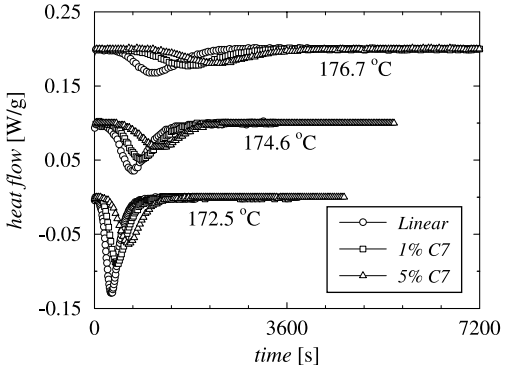

Fig. 4. Specific heat flux as a function of time during isothermal crystallizations at 172.5, 174.6 and 176.7 °C. Curves for the different temperatures have been shifted vertically for the sake of clarity.

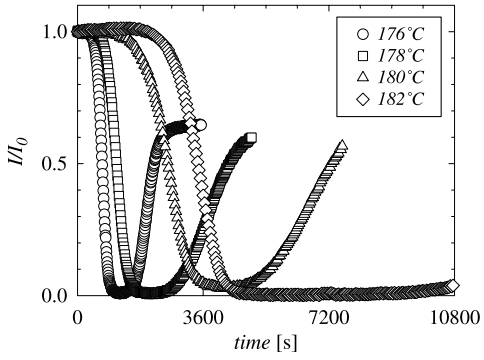

Fig. 5. Time evolution of relative light intensity during isothermal crystallization experiments for the 1% C7 sample. Different symbols refer to different crystallization temperatures.

scatters less light thus giving rise to a relative maximum (in the scattered light). A maximum in the scattered light, in turn, corresponds to a minimum in the transmitted light.

In order to follow the spherulitic radius as a function of time, V_H light scattering patterns were recorded and analyzed. The four-leaf patterns, characteristic of the arrangement of anisotropic crystallites within the spherulites, are clearly visible in Fig. 6. A quantitative analysis of the scattering patterns demonstrates that the intensity shows maxima at azimuthal angles of 45° and odd multiples. The scattering angle where the intensity is maximum, θ_{max}, and the average spherulitic radius, R, are linked by the following relation [35]:

$$4\pi\frac{R}{\lambda}\sin\left(\frac{\theta_{max}}{2}\right) = 4.0 \quad (5)$$

in which R is the average spherulitic radius, λ (=632.8 nm) is the wavelength of the laser light, and θ_{max} is the polar angle corresponding to the maximum intensity along a line of 45° to the polarization axes.

Data showing the spherulitic radius vs the crystallization time, as calculated form the SALS-pattern analysis, are reported in Fig. 7. Initially, the spherulite radius increases linearly with time; the slope in the linear region is the spherulitic growth rate G. After the linear region, the slope of the radius vs time curves drops to zero as a consequence of the spherulitic impingement. After the spherulitic impingement the spherulite radius remains constant but the intra-spherulitic crystallinity can still increase.

The average value of the final spherulitic radius for the 1% C7 sample is 24 μm. It should be noted that while the spherulitic dimension slightly increases with the crystallization temperature no systematic dependence upon the branching content could be observed. Optical microscopy observations confirm that the spherulitic radius at the end of the crystallization is of the order of 20 μm. The high nucleation density made difficult to obtain quantitative

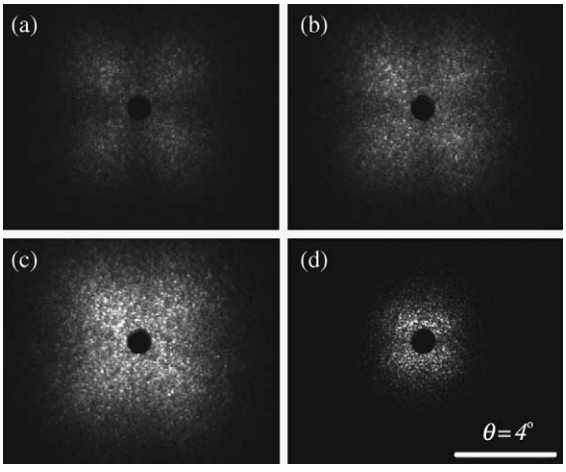

Fig. 6. Evolution of the VH scattering pattern during the isothermal crystallization at 176 °C of the linear PA11 sample. Snapshots at: (a) 16 min; (b) 18 min; (c) 20 min; (d) 48 min.

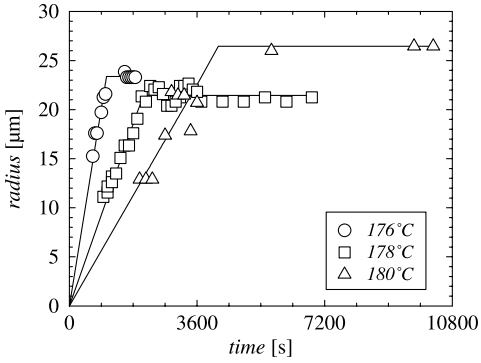

Fig. 7. Time evolution of the spherulitic radius during isothermal crystallization experiments for the 1% C7 sample. Different symbols refer to different crystallization temperatures.

measurements by means of optical microscopy whereas the analysis of the SALS patterns was still feasible. Comparison of Figs. 5 and 7 shows that when the spherulitic impingement occurs the corresponding intensity curve is in its minimum.

The spherulitic growth rate and the turbidity half-time as a function of the crystallization temperature and amount of branching are shown in Figs. 8 and 9, respectively. DSC half-crystallization times are also reported in Fig. 9. Figs. 8 and 9 clearly show that as the degree of branching decreases, the linear growth rate (Fig. 8) as well as the overall crystallization kinetics (Fig. 9) decrease. The 1% C7 sample has an overall crystallization rate and a spherulitic growth rate which are sensibly slower than those of the linear PA11 sample. The 5% C7 sample shows the slowest overall crystallization rate and the slowest spherulitic growth rate.

Since, the rheological behavior of all the samples is very similar, the observed differences in the crystallization kinetics cannot be explained by different mobilities of the polymeric chains in the liquid phase (note that the 5% C7 sample is the less viscous but the slowest to crystallize). Hence, we can certainly affirm that the small differences in the molecular masses cannot be responsible for the measured difference in the crystallization kinetics.

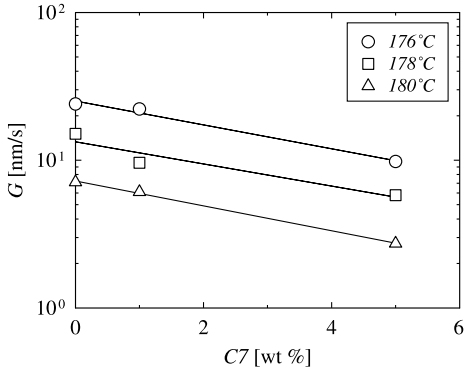

Fig. 8. Spherulitic growth rate vs amount of branches for the three PA11 samples. The solid lines through data points are linear regressions.

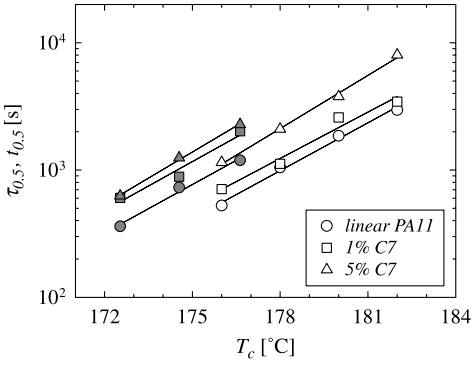

Fig. 9. Half-turbidity time vs crystallization temperature for the three PA11 samples. The solid lines through data points are linear regressions. Closed symbols are half-crystallization times form DSC measurements.

Short side branches are known not to enter the crystallites to any meaningful extent [36] thus reducing the sample crystallinity. This systematic crystallinity decrease, deduced from the DSC experiments, is indeed present in our samples, even for the less branched one.

It is remarkable that the half-crystallization time vs temperature curve and the half-turbidity time vs temperature curve run parallely and that the half-turbidity time is much lower than the half crystallization. These observations suggest that a very low crystallinity is sufficient to provoke a sensible opacification of the samples. Hence, when spherulitic impingement occurs, the crystallinity is still low. Much of the crystallinity develops after the spherulitic impingement as demonstrated by the fact that the samples' opacity is still changing when the final radius is already attained. This is most probably due to changes in intra-spherulitic crystallinity although this can only be investigated by an independent study of the crystallinity evolution in the system, a study that is outside the scope of this paper.

Both the half-crystallization time and the half-turbidity time increase with temperature following an Arrhenius-like behavior and the temperature coefficient is independent of the amount of C7 branches. The average value for the activation energy over the universal gas constant, E/R, is 60, 400 K; this value is similar to values from literature for PA11 [27].

3.3. Crystallization after shear flow

In this section, the effect of flow on the crystallization of the various PA11's is analyzed. Experiments were performed at a crystallization temperature of 180 °C. Shear rates of 0.1, 1, and 10 1/s (and strains of 6 and 60) were used. Materials were monitored optically (microscopy, SALS pattern, and transmitted light intensity) during and after the application of the flow.

Results for the half-turbidity time vs shear rate are shown in Fig. 10. They clearly show that the explored shear flow conditions do not affect the overall crystallization kinetics. Even for the strongest flow conditions ($\dot{\gamma} = 10$ 1/s, $\gamma = 60$) the half-turbidity times do not substantially differ from the quiescent values (which on Fig. 10 have been placed in correspondence of $\dot{\gamma} = 10^{-3}$ 1/s). The depolarized scattering patterns (not reported here) show the four-fold symmetry—with maxima at 45° and odd multiples—characteristic of undeformed spherulites. As already done for the quiescent conditions, spherulitic growth rates were calculated; also the spherulitic growth rates measured after the application of the shear deformation are substantially unaffected by the flow.

The crystallization rates of the highest molecular weight sample (the 1% C7) and of the most branched sample (the 5% C7) are both unaffected by the flow. The results are not completely surprising because polycondensation polymers have relatively narrow molecular weight distributions ($M_w/M_n \cong 2$) and relatively low molecular weights (few tens of g/mol). These two factors both contribute to extinguish the effect of flow upon the crystallization kinetics. In particular, for our polymers, the characteristic relaxation times at 180 °C, as extracted from the linear viscoelastic characterization, are: 0.6 s for the linear PA11; 2.1 s for the 1% C7; and 0.3 s for the 5% C7. The induction times for crystallization (at 180 °C) are in the order of a few thousand seconds for all the samples. These data suggest that some orientation is reached during the flow phase (Deborah numbers, defined as $De = \lambda_c \times \dot{\gamma}$, greater than unity are achieved), but this orientation is already fully relaxed when the crystallization sets in, thus providing the observed insensitivity of the overall crystallization kinetics to flow.

The fact that independently of the branching content not an increase of the crystallization kinetics can be observed was expected and in agreement with the rheological results. It is known that the presence of long chain branches greatly increases the polymers' relaxation times [33] thus producing a longer relaxation for the orientation (induced by a flow) and hence it enhances crystallization kinetics. The presence of short (C7) branches, in such small amounts, does not play any significant role in the polymer's linear viscoelastic behavior and consequently it produces no

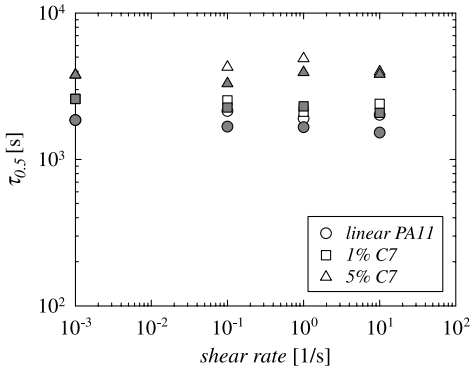

Fig. 10. Half-turbidity time vs shear rate, data refer to sheared samples. Open symbols refer to $\gamma = 6$, closed symbols refer to $\gamma = 60$.

relative differences in the crystallization kinetics under flow conditions.

4. Conclusions

The effect of short chain branches upon the quiescent and shear-stimulated crystallization of PA11 has been investigated in this paper.

The presence of short (C7) branches in small amounts (less than three branches per 1000 atoms in the main chain) do not affect the polymer linear viscoelastic behavior, where the only observed differences can be attributed to the different molecular weights.

The presence of C7-branches, even in the small amounts investigated, decreases the final crystallinity and substantially slows down the overall crystallization kinetics and the spherulitic growth rate.

The application of relatively strong shear conditions, up to $\dot{\gamma} = 10$ [1/s] and $\gamma = 60$, does not affect the crystallization behavior of linear and branched PA11; nucleation density and spherulitic growth rate do not show any increase due to the flow; and the crystallization occurs with spherulitic morphology under both quiescent and flow conditions.

Acknowledgements

S.A. thanks the Research Council of the Katholieke Universiteit Leuven for a postdoctoral fellowship. P.V.P. is indebted to the Fonds voor Wetenschappelijk Onderzoek-Vlaanderen (FWO)-Vlaanderen for a postdoctoral scholarship. We are thankful to Nino Grizzuti (University of Naples Federico II) for giving access to his DSC equipments and to H. Hennig Winter for a free license of IRIS. B. Ernst, N. Devaux and R. Linemann (Arkema, CERDATO) are acknowledged for the synthesis of the polyamides and the many useful discussions.

References

[1] Eder G, Janeschitz-Kriegl H. In: Meijer HEH, editor. Materials science and technology, vol. 18. Weinheim, Germany: Wiley-VCH Verlag GmbH; 1997. p. 269–342.
[2] Keller A, Cheng SZD. Polymer 1998;39(19):4461–87.
[3] Wilkinson AN, Ryan AJ. Polymer processing and structure development. Dordrecht, The Netherlands: Kluwer; 1998.
[4] Goschel U, Swartjes FHM, Peters GWM, Meijer HEH. Polymer 2000; 41(4):1541–50.
[5] Devaux N, Monasse B, Haudin JM, Moldenaers P, Vermant J. Rheol Acta 2004;43(3):210–22.
[6] Jerschow P, Janeschitz-Kriegl H. Int Polym Proc 1997;12(1):72–7.
[7] Kumaraswamy G, Kornfield JA, Yeh FJ, Hsiao BS. Macromolecules 2002;35(5):1762–9.
[8] Seki M, Thurman DW, Oberhauser JP, Kornfield JA. Macromolecules 2002;35(7):2583–94.
[9] Somani RH, Yang L, Hsiao BS. Physica A-Stat Mech Appl 2002; 304(1-2):145–57.
[10] Pogodina NV, Lavrenko VP, Srinivas S, Winter HH. Polymer 2001; 42(21):9031–43.
[11] Duplay C, Monasse B, Haudin JM, Costa JL. Polym Int 1999;48(4): 320–6.
[12] Acierno S, Grizzuti N, Winter HH. Macromolecules 2002;35(13): 5043–8.
[13] Acierno S, Palomba B, Winter HH, Grizzuti N. Rheol Acta 2003; 42(3):243–50.
[14] Elmoumni A, Winter HH, Waddon AJ, Fruitwala H. Macromolecules 2003;36:6453–61.
[15] Lohse DJ, Milner ST, Fetters LJ, Xenidou M, Hadjichristidis N, Mendelson RA, et al. Macromolecules 2002;35(8):3066–75.
[16] Vega JF, MunozEscalona A, Santamaria A, Munoz ME, Lafuente P. Macromolecules 1996;29(3):960–5.
[17] Agarwal PK, Somani RH, Weng WQ, Mehta A, Yang L, Ran SF, et al. Macromolecules 2003;36(14):5226–35.
[18] Mandelkern L. Phyiscal properties of polymers. 2nd ed. Washington DC: American Chemical Society; 1993.
[19] Ward IM, Hadley D. Mechanical properties of solid polymers. 2nd ed. New York: Wiley; 1993.
[20] Jordens K, Wilkes GL, Janzen J, Rohlfing DC, Welch MB. Polymer 2000;41(19):7175–92.
[21] Bensason S, Minick J, Moet A, Chum S, Hiltner A, Baer E. J Polym Sci, Part B: Polym Phys 1996;34(7):1301–15.
[22] Nunes RW, Martin JR, Johnson JF. Polymer 1982;22(4):205–28.
[23] Kale LT, Plumley TA, Patel RM, Redwine OD, Jain P. J Plast Film Sheeting 1996;12(1):27–40.
[24] Simanke AG, Galland GB, Neto RB, Quijada R, Mauler RS. J Appl Polym Sci 1999;74(5):1194–200.
[25] Liu M, Zhao Q, Wang Y, Zhang C, Mo Z, Cao S. Polymer 2003;44(8): 2537–45.
[26] Zhang Q, Mo Z, Liu S, Zhang H. Macromolecules 2000;33(16): 5999–6005.
[27] Liu S, Yu Y, Cui Y, Zhang H, Mo Z. J Appl Polym Sci 1998;70: 2371–80.
[28] Khanna YP, Han PK, Day ED. Polym Eng Sci 1996;36(13):1754.
[29] Laun HM. Rheol Acta 1979;18(4):478–91.
[30] Acierno S, Van Puyvelde P. J Appl Polym Sci 2005;97:666–70.
[31] Blondel P, Briffaud T, Werth MRG. Macromol Symposia 1997;122: 243–8.
[32] Jaques B, Werth M, Merdas I, Thominette F, Verdu J. Polymer 2002; 43:6439–47.
[33] Ferry JD. Viscoelastic properties of polymers. 3rd ed. New York: Wiley; 1980.
[34] Baumgaertel M, Winter HH. Rheol Acta 1989;28(6):511–9.
[35] Stein RS, Rhodes MB. J Appl Phys 1960;31(11):1873–84.
[36] Strobl GR. The physics of polymers: Concepts for understanding their structures and behavior. 2nd ed. Berlin: Springer; 1997.